The Protein Backbone Makes Important Contributions to 4-Oxalocrotonate Tautomerase Enzyme Catalysis: Understanding from Theory and Experiment†

G. Andrés Cisneros, Min Wang, Peter Silinski,‡ Michael C. Fitzgerald,* and Weitao Yang*

Department of Chemistry, Duke University, Durham, North Carolina 27708-0346

Received January 8, 2004; Revised Manuscript Received March 26, 2004

ABSTRACT: The role of polypeptide backbone interactions in 4-oxalocrotonate tautomerase (4OT) catalysis has been investigated using a combination of site-directed mutagenesis experiments with unnatural amino acids and quantum mechanical/molecular mechanical (QM/MM) calculations of the 4OT reaction mechanism. Energy barriers for the wild-type enzyme (wt-4OT) and for a 4OT analogue containing a backbone amide to ester bond mutation between Ile-7 and Leu-8 [(OL8)4OT] were determined by both theory and experiment. The amide to ester bond mutation in (OL8)4OT effectively deleted a putative hydrogen bonding interaction between the enzyme's polypeptide backbone and its substrate. Recent theoretical calculations for the 4OT reaction mechanism suggested that this hydrogen bonding interaction helps properly position the substrate in the active site [Cisneros, G. A., *et al.* (2003) *J. Am. Chem. Soc. 125*, 10384−10393]. Our experimental results for (OL8)4OT reveal that the energy barrier for the (OL8)-4OT-catalyzed reaction was increased 1.8 kcal/mol over that of the wild-type enzyme. This increase was in good agreement with the 1.0 kcal/mol increase obtained from QM/MM calculations for this analogue. Our theoretical calculations further suggest the hydrogen bond deletion in (OL8)4OT results in a rearrangement of the substrate in the active site. In this rearrangement, an ordered water molecule loses its ability to stabilize the transition state (TS), and Arg-61 gains the ability to stabilize the TS. The predicted role of Arg-61 in (OL8)4OT catalysis was confirmed in kinetic experiments with an analogue of (OL8)-4OT containing an Arg to Ala mutation at position 61.

Interactions involving the polypeptide backbone of proteins can play important roles in protein folding and function (*1*). Theoretical calculations (*2*) on model systems have suggested that hydrogen bonding interactions involving backbone amide groups can stabilize enzyme−substrate complexes, and experimental investigations (*3*) utilizing unnatural amino acid mutagenesis techniques have helped substantiate the hypothesis that hydrogen bonding interactions involving the peptide backbone can contribute to protein folding and function. However, while several different protein systems have been subjected to such theoretical and experimental analyses, to our knowledge there has been no study of backbone interactions and enzyme catalysis in which theory and experiment have been applied to the same protein system. Here we use a total chemical synthesis strategy to understand the role of the protein backbone in the catalytic mechanism of 4-oxalocrotonate tautomerase (4OT),[1] and we compare these experimental results with theoretical simulations of the enzyme's reaction mechanism.

4OT is a homohexameric bacterial enzyme that catalyzes the ketonization of both 2-hydroxymuconate (2HM) and 2-oxo-4-hexenedioate (2o4hex) to 2-oxo-3-hexenedioate (2o3hex) (see Figure 1) (*4*). A recent theoretical study of 4OT's catalytic properties implicated a hydrogen bond between the backbone NH group of Leu-8 and the substrate 2-oxo-4-hexenedioate in the enzymatic reaction (*5*). The X-ray crystal structure of 4OT (*6*) shows that the backbone NH group of Leu-8 is located very close to the active site of the enzyme at the end of a β-strand near the major subunit interface. On the basis of the results from these earlier theoretical and structural studies on 4OT, we designed a set of experiments to elucidate the role of the backbone NH group of Leu-8 in 4OT's catalytic mechanism.

As part of this work, we prepared a synthetic 4OT analogue, (OL8)4OT, in which the amide bond between Ile-7 and Leu-8 was replaced with an ester bond. This mutation was designed to effectively delete a putative backbone hydrogen bond interaction between the NH group of Leu-8 and the substrate. Our experimental results indicate that the structural and catalytic properties of (OL8)4OT were nearly identical to those of the wild-type enzyme with the exception

† This work was supported by NIH grants to M.C.F. and W.Y. (Grants RO1 GM61680 and RO1 GM61871, respectively). G.A.C. thanks CONACyT for partial financial support.

* To whom correspondence should be addressed. M.C.F.: Duke University, Durham, NC 27708-0346; telephone, (919) 660-1547; fax, (919) 660-1605; e-mail, michael.c.fitzgerald@duke.edu. W.Y.: Duke University, Durham, NC 27708-0346; telephone, (919) 660-1562; fax, (919) 660-1605; e-mail, weitao.yang@duke.edu.

‡ Present address: Trimeris Inc., Durham, NC 27707.

[1] Abbreviations: 4OT, 4-oxalocrotonate tautomerase; 2HM, 2-hydroxymuconate; 2o4hex, 2-oxo-4-hexenedioate; 2o3hex, 2-oxo-3-hexenedioate; GuHCl, guanidine hydrochloride; UV−CD, ultraviolet−circular dichroism; SEC, size-exclusion chromatography; RP-HPLC, reversed-phase high-performance liquid chromatography; ESI-MS, electrospray ionization mass spectrometry; QM/MM, quantum mechanical/molecular mechanical; rmsd, root-mean-square deviation; SPPS, solid-phase peptide synthesis; HF/3-21G, Hartree−Fock with the 3-21G basis set; B3LYP/6-31G*, Becke 3 exchange and Lee, Yang, Parr correlation with the 6-31G* basis set.

10.1021/bi049943p CCC: $27.50
Published on Web 05/11/2004

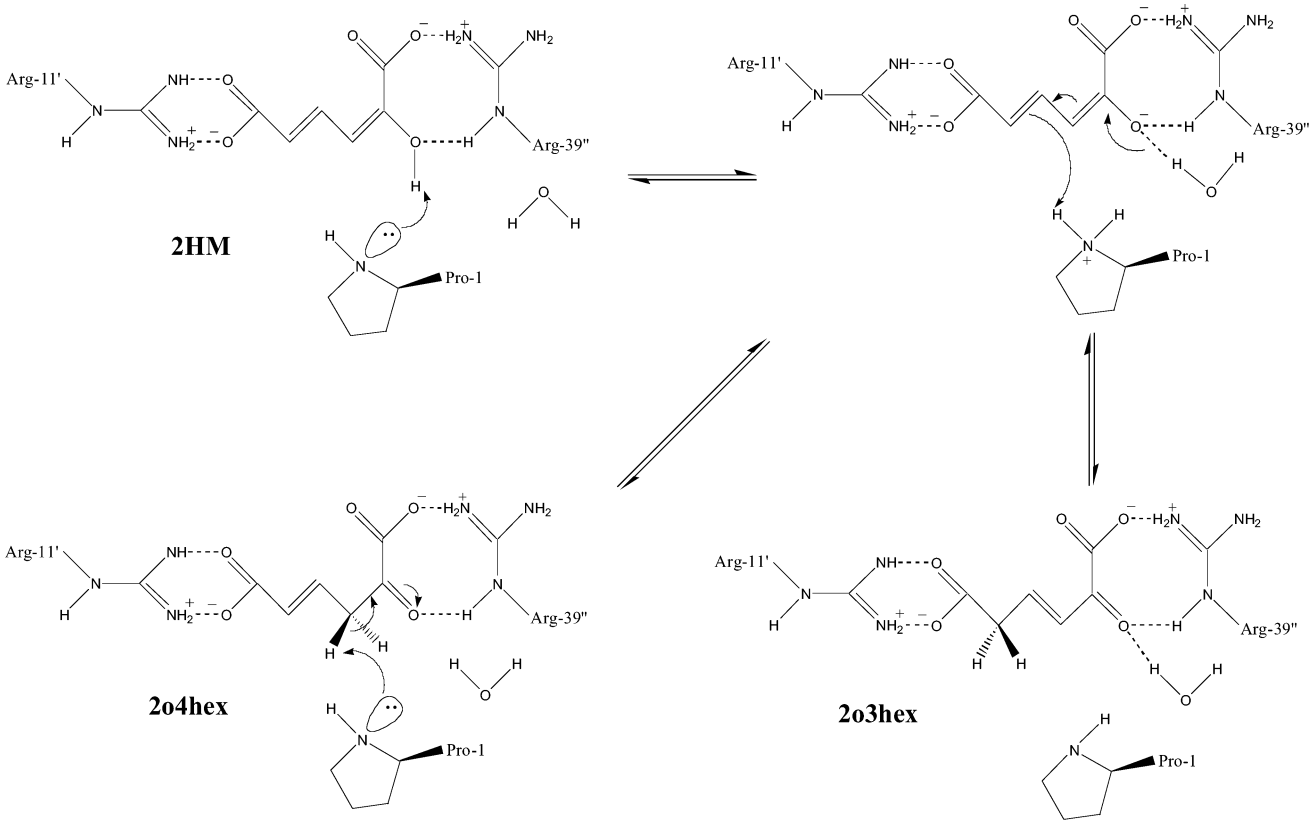

FIGURE 1: Proposed mechanism for 4OT catalysis (*5*, *12*).

that the k_{cat} for (OL8)4OT was reduced approximately 20-fold compared to that of the wild-type enzyme. This reduction in k_{cat} can be equated with a 1.8 kcal/mol increase in the energy barrier for the enzymatic reaction, and it is consistent with the 1.0 kcal/mol increase in the energy barrier for the enzymatic reaction predicted from our QM/MM calculations on (OL8)4OT. Moreover, our theoretical calculations on (OL8)4OT suggested that the hydrogen bond deletion in (OL8)4OT results in a rearrangement of the substrate in the active site. As part of this rearrangement, Arg-61 gains the ability to stabilize the TS in (OL8)4OT catalysis. This was confirmed in experiments on a second synthetic analogue of 4OT in which the amide bond between Ile-7 and Leu-8 was replaced with an ester bond and in which Arg-61 was replaced with an Ala.

MATERIALS AND METHODS

Materials. The *tert*-butoxycarbonyl (Boc) L-amino acids were purchased from Peptide Institute, Inc., and Novabiochem, and *tert*-Boc-Arg(tosyl) OCH_2 PAM resin was obtained from Applied Biosystems. L-2-Hydroxyisocaproic acid (OLeu), *N*,*N*-diisopropylethylamine, diisopropylcarbodiimide, and *N*-ethylmorpholine were purchased from Sigma-Aldrich. L-(+)-Lactic acid was purchased from Fluka. 2-(1*H*-Benzotriazol-1-yl)-1,1,3,3-tetramethyluronium hexafluorophosphate (HBTU) was obtained from Quantum Biotechnologies. Neat trifluoroacetic acid (biograde) was purchased from Halocarbon, and spectroscopic grade dimethylformamide was obtained from J. T. Baker. Anhydrous HF (UHP) was purchased from Matheson Gas. HPLC grade acetonitrile was purchased from Mallinckrodt. All other chemicals were reagent grade or better.

Experimental Methods and Instrumentation. Analytical and preparative reversed-phase high-performance liquid chromatography (RP-HPLC) separations were performed on a Rainin instrument consisting of a Dynamax SD-200 solvent delivery system and a Dynamax variable-wavelength UV−visible absorbance detector. Analytical RP-HPLC was performed on a C_{18} Vydac column (0.46 cm × 15.0 cm, 300 Å) at a flow rate of 1 mL/min. Preparative RP-HPLC was performed on a C_{18} Vydac column (2.2 cm × 12.0 cm, 300 Å) at a flow rate of 10 mL/min. All RP-HPLC separations were performed using linear gradients of buffer B in buffer A (buffer A consisting of 0.1% TFA in water and buffer B of 90% acetonitrile in water containing 0.09% TFA). Detection for analytical and preparative separations was at 214 and 230 nm, respectively. Size-exclusion chromatography (SEC) was also performed on the Dynamax system using a Superdex 75 HR 10/30 column (Pharmacia Biotech) at a flow rate of 1 mL/min. The mobile phase was 20 mM sodium phosphate buffer (pH 7.0), and the detector was set at 214 nm.

ESI-MS spectra were obtained using a PE-Sciex API 150EX instrument. Samples were typically diluted into 40% buffer B in buffer A, and then infused directly into the mass spectrometer at a flow rate of 10 μL/min using a Harvard syringe pump. All far-UV−CD measurements were performed on a Jasco-710 spectropolarimeter. Spectra were acquired at 25 °C using a bandwidth of 0.5 nm. All UV−vis absorbance data were collected using a Hewlett-Packard 8452A diode array UV−vis spectrophotometer. All far-UV−CD data were acquired using a quartz cuvette (1 mm). UV−vis absorbance spectra were acquired using quartz cuvettes with path lengths of either 1.0 cm or 1.0 mm. Enzyme

concentrations were determined using the Waddell method (*7*).

Peptide Synthesis and Purification. The two synthetic 4OT constructs in this study were both prepared by total chemical synthesis using manual solid-phase peptide synthesis (SPPS) methods and *in situ* neutralization protocols for Boc chemistry as described elsewhere (*8*). Each synthesis was initiated on Boc-L-Arg(tosyl) OCH_2 PAM resin. Side protection was as follows: Arg(Tos), Asp(OcHex), Glu(OcHex), His(Bom), Lys(2-Cl-Z), Ser(Bzl), and Thr(Bzl) where Tos is tosyl, OcHex is cyclohexyl, Bom is *tert*-butyloxymethyl, 2-Cl-Z is 2-chlorobenzyloxycarbonyl, and Bzl is benzyl. Side chain deprotection and cleavage of the peptide from the resin were carried out by treatment with anhydrous HF at 0 °C for 1 h. Following removal of HF under reduced pressure, the crude peptide product from each synthesis was precipitated and washed with cold anhydrous diethyl ether, dissolved in a minimal amount of 70% acetonitrile containing 0.1% TFA, diluted with water, frozen, and lyophilized. The desired product form was purified by preparative RP-HPLC using a 40 to 60% linear gradient of buffer B in buffer A. Pure RP-HPLC fractions, as judged by ESI-MS analysis, were pooled, frozen, and lyophilized to a dry, white solid.

The ester bonds in (OL8)4OT and (OL8)4OT(R61A) were incorporated into the polypeptide backbones of these two proteins by coupling L-2-hydroxyisocaproic acid (OLeu) instead of L-leucine at position 8 according to a previously established protocol (*3b*). The appropriate Boc-protected amino acid was coupled to the OLeu residue for 1 h according to a previously reported protocol (*3b*), and this coupling procedure was repeated twice to increase the coupling yield. The (OL8)4OT analogue also contained a methionine to norleucine mutation at position 45 in 4OT's polypeptide chain.

Protein Folding Protocol. The pure, lyophilized product from each synthesis was folded as described previously.[3g] Briefly, ~0.5−1.0 mg of the RP-HPLC-purified product from each synthesis was dissolved in 10−20 μL of 50 mM phosphate buffer (pH 7.0) containing 5.0 M guanidine hydrochloride (GuHCl). The resulting protein solution was diluted at least 50-fold into 50 mM phosphate (pH 7.0), and each protein was allowed to refold for 1 h at room temperature. Any insoluble material was pelleted by ultracentrifugation prior to analysis by SEC. The folded hexamers were further purified by SEC, concentrated using Microcon YM-3 centrifugal filter devices, and analyzed by far-UV−CD spectroscopy and catalytic activity measurements.

Catalytic Activity Measurements. The catalytic activities of the (OL8)4OT and (OL8)4OT(R61A) analogues were assayed using the substrate 2HM as described previously (*3g*). Briefly, this was accomplished by monitoring the change in absorbance at 232 nm, corresponding to the rate of product formation. For each rate, absorbance data were collected in 1 s intervals over a time period of 5 s, and the catalytic rate was determined in absorbance units per second by linear least-squares analysis of the raw data. In each activity assay, the final concentration of the enzyme was 1−50 nM, and the final concentration of the substrate was 20−400 μM. All activity measurements were recorded in 20 mM phosphate buffer (pH 7.0), and measurements were recorded in triplicate at multiple concentrations of 2HM. In accordance with Michaelis−Menten enzyme kinetics, these rates were used to create Lineweaver−Burk plots, and linear-least squares analyses of these plots of 1/rate versus 1/[2HM] were ultimately used to calculate k_{cat} and K_M values in triplicate.

Computational Methods. QM/MM calculations were performed on a (OL8)4OT enzyme−substrate complex and on the wild-type enzyme−substrate complex. The initial structures of the enzyme−substrate complexes used in our calculations were identical to those for the reactant structure for wild-type 4OT (wt-4OT) determined in our previous work (*5*). Briefly, the initial structure of inactivated wt-4OT was taken from the Protein Data Bank (1BJP); the inhibitor was replaced with the substrate, and MD simulations and QM/MM optimizations were performed to relax the structure and obtain an initial enzyme−substrate complex. For the initial structure of (OL8)4OT, the NH group of Leu-8 was replaced with an O atom on all six monomers, resulting in six atoms being removed overall. We also note that in this case both wt-4OT and (OL8)4OT included 2HM as the substrate for comparison with the experimental determinations presented here, not 2o4hex as in our previous study (*5*).

In all cases, the QM subsystem consisted of 36 atoms that include Pro-1, the substrate molecule, and a water molecule (H_2O-1); the rest of the enzyme and the solvation (water) sphere were located in the MM subsystem to give a total of 13 197 atoms in wt-4OT and 13 191 atoms in (OL8)4OT. All MM calculations were performed using the criteria for convergence and methodology, as well as using the programs developed in our previous study of the wild-type enzyme (*5*). All energy paths were calculated with a modified version of Gaussian98 that interfaces with a modified version of TINKER (*9*).

The initial structures generated for the wild-type enzyme and (OL8)4OT analogue were minimized and subjected to a 200 ps MD equilibration. The overall rmsd between the crystal structure and the calculated ground state structures was less than 1.0 Å for both structures. After the reactant structures were obtained, the reaction paths were determined by means of the reaction coordinate driving method (RCDM) (*10*) for both steps of the wt-4OT and (OL8)4OT reaction mechanisms.

In all cases, the geometries for each point in the paths were optimized at the HF/3-21G level, and subsequently, a single-point calculation at the B3LYP/6-31G* level was performed, as well as single-point calculations at the B3LYP/6-311G** level for the stationary points only. Frequency calculations were performed for the structures located on the maxima and minima along the paths. Reactants, products, and intermediates were characterized as not having any negative frequencies. All TSs were found to be maxima exclusively along the reaction coordinate and minima along all other directions, and also presented only one negative frequency (see the Supporting Information).

Once the structures in the reaction path were determined, it was possible to dissect the contributions of individual residues to catalysis by breaking down the energy into contributions per residue in a perturbative way. This perturbative analysis was carried out by breaking the energy barriers into components and considering only the changes in electrostatic contributions. The interaction energies between individual residues and the QM subsystem when the enzyme moves from the reactant state to TSs are calculated

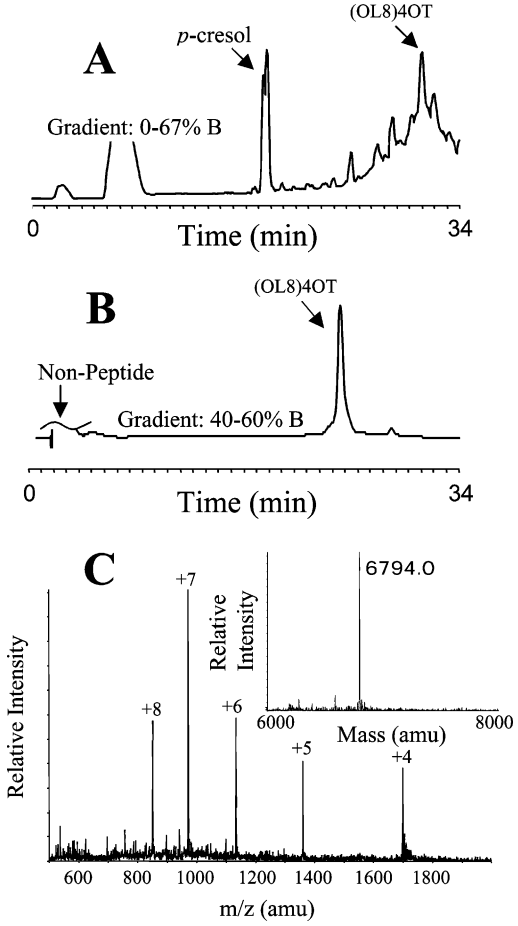

FIGURE 2: RP-HPLC and ESI-MS analysis of (OL8)4OT synthesis. (A) RP-HPLC of the (OL8)4OT crude product mixture after HF cleavage. The major peak at approximately 31 min corresponds to the full-length 62mer. (B) Analytical RP-HPLC of (OL8)4OT after purification by RP-HPLC. The major peak at approximately 24 min is the purified 62mer. (C) ESI-MS of material collected from the 24 min peak in the chromatogram shown in panel B. The multiple charge states are labeled next to each ion signal corresponding to (OL8)4OT, and the inset shows the reconstruction of the raw MS data along with the calculated mass.

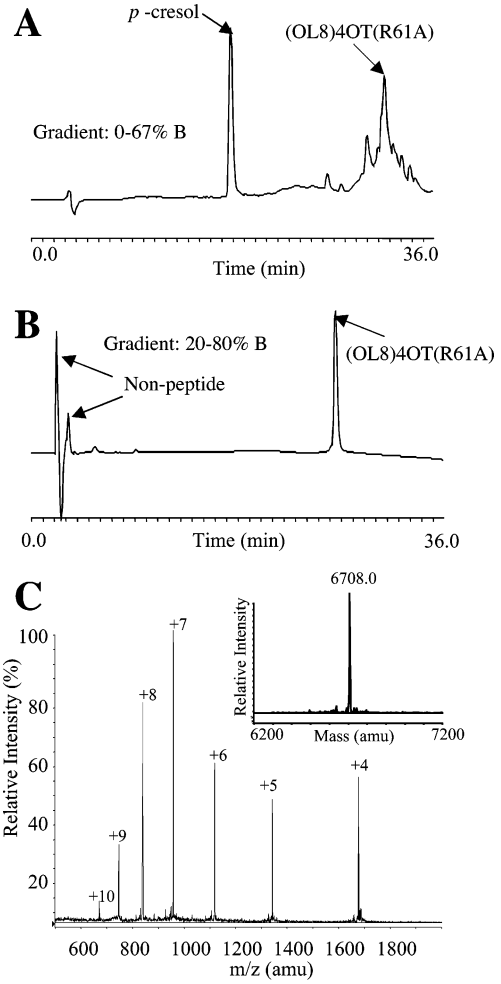

FIGURE 3: RP-HPLC and ESI-MS analysis of (OL8)4OT(R61A) synthesis. (A) RP-HPLC of the crude product mixture after HF cleavage. The major peak at approximately 31 min corresponds to the full-length 62mer. (B) Analytical RP-HPLC of (OL8)4OT-(R61A) after purification by RP-HPLC. The major peak at approximately 26 min is the purified 62mer. (C) ESI-MS of material collected from the 26 min peak in the chromatogram shown in panel B. The multiple charge states are labeled next to each ion signal corresponding to (OL8)4OT(R61A), and the inset shows the reconstruction of the raw MS data along with the calculated mass.

by averaging the electrostatic interaction energies between the residues and the QM subsystem for an ensemble of structures (generally 50), where the conformational space of the MM part is sampled to obtain the free energy contribution. This defines the perturbative anlaysis we describe in our results.

RESULTS AND DISCUSSION

Chemical Synthesis and Characterization of (OL8)4OT and (OL8)4OT(R61A). The 62-amino acid polypeptide chains of (OL8)4OT and (OL8)4OT(R61A) were readily assembled by SPPS and easily purified by RP-HPLC (see Figures 2 and 3). The (OL8)4OT and (OL8)4OT(R61A) constructs in this work both contained a methionine to norleucine mutation at position 45 in 4OT's polypeptide chain. This mutation was incorporated into our synthetic constructs to eliminate the possibility of side chain oxidation during synthesis and purification. We have previously shown that this mutation does not alter the structural or catalytic properties of the enzyme (*11*). Our previous calculations on the wild-type enzyme also showed that Met-45 does not contribute to 4OT catalysis (*5*). The catalytic properties of the synthetic constructs prepared in this work were ultimately compared to those we have previously reported for 4OT(N).

The RP-HPLC-purified synthetic products obtained from the total chemical syntheses of (OL8)4OT and (OL8)4OT-(R61A) were folded and analyzed by SEC (Figure 4). The SEC chromatograms we obtained for (OL8)4OT, (OL8)4OT-(R61A), and the synthetic wild-type control, 4OT(N), included peaks at 11, 13, 17, and 21.5 min. The retention time of the 11 min peak is consistent with that expected for the native 4OT hexamer, and the small amount of GuHCl that is carried over from the protein folding protocol elutes in the 21.5 min peak. The 13 and 17 min peaks are similar to those observed in our earlier SEC studies on other ester bond-containing analogues of 4OT. The polypeptide material that elutes in the 13 and 17 min peaks apparently adopts a non-native-like, partially folded structure, as judged by far-UV−CD analysis (data not shown). The relative amount of polypeptide material that elutes in the 13 and 17 min peaks appears to be related to the folding yields of our synthetic constructs and not the presence of different equilibria. Evidence supporting this conclusion comes from the fact that

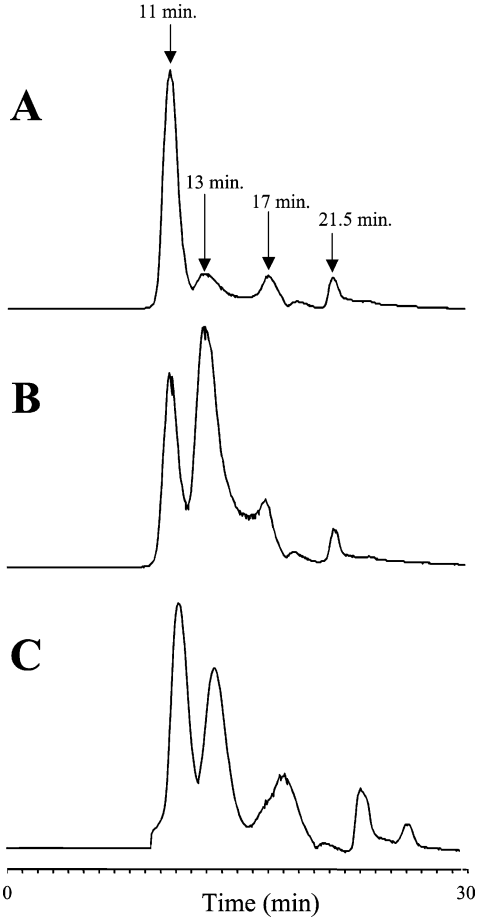

FIGURE 4: SEC analysis of 4OT analogues in 20 mM phosphate buffer at pH 7.0 and 25 °C: (A) 4OT(N), (B) (OL8)4OT, and (C) (OL8)4OT(R61A). Peaks with retention times of 11 min correspond to folded 4OT hexamers, and peaks with retention times of 13 and 17 min correspond to non-native material. Peaks with retention times of 21.5 min correspond to GuHCl.

when material isolated from the 11 min peak in the (OL8)-4OT and (OL8)4OT(R61A) chromatograms was collected, allowed to equilibrate for 5 h, and reanalyzed by SEC, only a single peak at 11 min was observed (data not shown).

Shown in Figure 4 is the far-UV−CD spectra recorded for material isolated in the 11 min SEC peaks of the 4OT-(N), (OL8)4OT, and (OL8)4OT(R61A) samples. The three spectra in Figure 4 are nearly identical and consistent with spectra previously reported for the wild-type enzyme. These results suggest that the ester bond mutations in (OL8)4OT and (OL8)4OT(R61A) do not dramatically alter 4OT's native, three-dimensional structure. The k_{cat} and K_M values determined for the material isolated in the 11 min peak of the SEC chromatogram of the (OL8)4OT and (OL8)4OT-(R61A) constructs are presented in Table 1 along with similar values previously reported for 4OT(N) and for a 4OT(R61A) construct. While no error was reported in ref *3g* for the kinetic parameters of 4OT(N), it is expected that the relative standard deviation of these measurements is comparable to that of our measurements on (OL8)4OT and (OL8)4OT-(R61A) (i.e., ±20−30%).

The experimental data in Table 1 indicate that the k_{cat} of (OL8)4OT is reduced 20-fold compared to that of 4OT(N) and that the k_{cat} of (OL8)4OT(R61A) is reduced 8-fold compared to that of (OL8)4OT. These results suggest that the replacement of the native backbone amide bond between

Table 1: Catalytic Activity Parameters of 4OT Analogues

analogue	k_{cat} (s^{-1})	K_M (μM)	$\Delta\Delta G^{\ddagger}_{exp}$ (kcal/mol)	$\Delta\Delta E^{\ddagger}_{theor}$ (kcal/mol)
4OT(N)	1600[a]	93[a]	*c*	*c*
(OL8)4OT	80 ± 20[b]	270 ± 110[b]	1.8	1.0
(OL8)4OT(R61A)	11 ± 3[b]	128 ± 40[b]	1.2[d]	1.5[e]

[a] Data taken from ref *3g*. [b] Errors are ±1 standard deviation. [c] Not available. [d] Energy difference taken with respect to (OL8)4OT (see the text). [e] Energy difference calculated from perturbative analysis on (OL8)4OT (see the text and Table 2).

Ile-7 and Leu-8 with an ester bond significantly decreases the catalytic efficiency of 4OT. These results also indicate that Arg-61 contributes to the catalytic properties of (OL8)-4OT. This is in contrast to the nonexistent role that Arg-61 has been shown to play in the catalytic properties of the wild-type enzyme (*12b*).

We have previously reported on the chemical synthesis and biophysical characterization of two additional ester bond-containing 4OT analogues (*3g*), and we currently have preliminary data on the structure and function of eight additional ester bond-containing 4OT analogues in which the ester bond mutation was introduced into a series of different backbone positions in the β-sheet and α-helical regions of 4OT's three-dimensional structure (*13*). We note that of a total of seven ester bond-containing 4OT analogues that have been prepared and found to fold into a native-like hexamer, the (OL8)4OT analogue was the only analogue with altered catalytic properties.

To date, the catalytic contributions of three major residues in 4OT's primary amino acid sequence (i.e., Pro-1, Arg-11, and Arg-39) have been elucidated. There is substantial biochemical evidence suggesting that Pro-1 is the general base catalyst. An unnatural amino acid-containing analogue of 4OT in which Pro-1 was replaced with cyclopentane-carboxylate displayed no measurable catalytic acitivity (i.e., $k_{cat} < 1\ s^{-1}$) (*11*). Alanine substitutions at Arg-11 and Arg-39 resulted in decreased k_{cat} values that were 19- and 140-fold smaller, respectively, than the k_{cat} value of the wild-type enzyme (*12*). The overall catalytic efficiencies (i.e., k_{cat}/K_M values) of these two alanine-containing 4OT analogues were decreased 20- and 170-fold, respectively. In comparison, the k_{cat}/K_M values for (OL8)4OT and (OL8)4OT(R61A) were decreased 57- and 160-fold, respectively, compared to that of our synthetic wild-type control, 4OT(N).

Theoretical Calculations. The 4OT reaction mechanism was modeled as a two-step process. The first step was defined by the abstraction of a proton from the 2HM substrate by Pro-1, and the second step was defined by the transfer of this proton from Pro-1 back to the substrate to form the final product in the isomerization reaction, 2-oxo-3-hexenedioate. The B3LYP/6-31G* energy barriers for the first step of the reaction mechanism are 8.19 kcal/mol for the wild type and 15.47 kcal/mol for (OL8)4OT (Supporting Information). If a 6-311G** basis set is used in the calculations, the energy barriers for the first step are 7.47 and 16.71 kcal/mol for the wild-type and (OL8)4OT construct, respectively. In the second step, the calculated B3LYP/6-31G* energy barriers for the wild type and (OL8)4OT mutant are 14.47 and 15.17 kcal/mol, respectively (or 16.98 and 19.76 kcal/mol, respectively, if the 6-311G** basis set is used).

The differences between the rate-limiting barriers, for the wild type and the (OL8)4OT analogue, yield a $\Delta\Delta E$ value of 1.0 using the 6-31G* basis set and a $\Delta\Delta E$ value of 2.8 kcal/mol using the 6-311G** basis set in the calculations. We note that the second step was the rate-limiting step for both the wild type and (OL8)4OT when the 6-311G** basis set was used, but when the 6-31G* basis set was employed, the first step in the (OL8)4OT reaction became rate-limiting. The rate-limiting step of the wild-type reaction was unchanged when the 6-31G* basis set was used. Significantly, the $\Delta\Delta E$ values calculated above are in reasonably good agreement with the $\Delta\Delta G^{\ddagger}$ value of 1.8 kcal/mol that can be derived with transition state theory using our experimentally determined difference in k_{cat} values between 4OT(N) and (OL8)4OT. However, we note that the inclusion of a zero-point energy correction at the Hartree−Fock level yields a $\Delta\Delta E$ value of 4.3 kcal/mol at the B3LYP/6-31G* level of theory or 3.02 at the B3LYP/6-311G** level of theory (see the Supporting Information).

It is important to note that the reaction mechanism for both native and mutant structures proceeds through a general acid−base mechanism; however, there is no general acid *per se*, in agreement with our previous results (see Figure 1) (*5*). In both cases, the negative charge that is formed in the intermediate and transition state structures is stabilized via electrostatic interactions from Arg-39″ and an ordered water in the active site, labeled H_2O-2, without a proton transfer to the oxygen on C2 of the substrate. In our notation, as in our previous work (*5*), the unprimed and singly primed residues belong to two different monomers of the same dimer, and the doubly primed residue belongs to a third monomer.

A comparison between the calculated reactant structures of wt-4OT and (OL8)4OT helps explain (OL8)4OT's reduced catalytic activity. Specifically, the amide to ester bond mutation in the (OL8)4OT analogue produces a slight rearrangement of the substrate in the active site with respect to wt-4OT. In wt-4OT, the substrate forms a H-bond with the backbone NH group of Leu-8, as well as a H-bond with Arg-61′ (Figures 6A and 7A). Arg-61′ also forms a H-bond to a water molecule (labeled H_2O-2) which permits this water to approach the carbonyl site and stabilize the negative charge that is formed in the TSs (*5*). In (OL8)4OT, the mutation removes the backbone H-bond, which causes a rearrangement of the substrate in the active site and allows the formation of a second H-bond between the substrate and Arg-61′ (Figures 6B and 7B). The formation of this second H-bond forces H_2O-2 to change its position in the active site, rendering this water molecule unavailable for the stabilization of the negative charge in the TSs.

In Table 2, we present a comparison of the residues and water molecules that present a significant change in (de)-stabilization of the TS in (OL8)4OT with respect to the wild type. Other residues that are important to TS stabilization have been discussed in our previous work (*5*). These residues for both structures with important contributions, which do not change between wt-4OT and (OL8)4OT, are discussed in the Supporting Information. It is important to note that the energy breakdowns in Table 2 and in the Supporting Information can be seen as only a first-order approximation to the contribution of the residues to the TS stabilization, and therefore, the results are only qualitative, as has been

Table 2: Electrostatic Contributions to TS Stabilization for Selected Residues with a Significant Change between wt-4OT and (OL8)4OT (see the text)[a]

	first step		second step	
residue	wild type[b]	(OL8)4OT	wild type	(OL8)4OT
Leu-8′	−0.90	−0.32	−1.33	−0.57
Arg-61′	−0.26	−1.54	−0.36	−1.22
H_2O-2	−1.99	−0.01	−2.14	−0.42
H_2O-5	−0.17	−1.87	−0.17	−2.07

[a] A summary of all the (de)stabilization data that were collected is provided in the Supporting Information. A negative value means that this residue stabilizes the TS, while a positive value means that this residue destabilizes the TS. [b] Values for the first-step stabilization correspond to the highest value obtained between both TSs in the first step (Supporting Information).

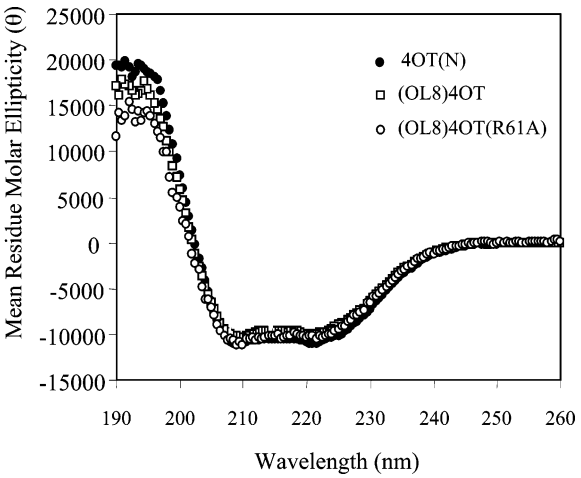

FIGURE 5: Far-UV−CD analysis of 4OT analogues at pH 7.0 and 25 °C. The spectra for 4OT(N) (●), (OL8)4OT (□), and (OL8)-4OT(R61A) (○) were acquired using a quartz cuvette with a path length of 1 mm, and the protein concentration was approximately 30 μM.

previously explained (*5*). This is in contrast to our quantitative QM/MM calculations on the wild-type enzyme and on the (OL8)4OT analogue that lead to the calculation of a specific $\Delta\Delta E$ value for the amide to ester bond mutation in (OL8)4OT, although it is interesting to note that the 1.3 kcal/mol contribution of Leu-8 predicted in our perturbative calculations is in reasonably good agreement with that predicted in our QM/MM calculations, 1.0 kcal/mol.

Significantly, a qualitative analysis of the H_2O-2 data in Table 2 supports a reaction scheme for the wild-type enzyme in which a water molecule helps to stabilize the negative charge formed in the TS without acting as a general acid (*5*). Interestingly, the data in Table 2 show that such a water is not involved in the reaction scheme for (OL8)4OT. In the case of wild-type 4OT, H_2O-2 contributes approximately 2 kcal/mol of stabilization to both steps of the reaction. For (OL8)4OT, this water molecule's contribution is significantly reduced. Moreover, while another water molecule, H_2O-5, was found to contribute to the stabilization for (OL8)4OT (see Table 2 and Figure 6), it was found that this water molecule is not in a position to help stabilize the negative charge, resulting in an increase in the energy barrier. No other water molecules were found to be available to stabilize the negative charge.

Another important theoretical result from the calculations summarized in Table 2 is that Arg-61′ does not significantly

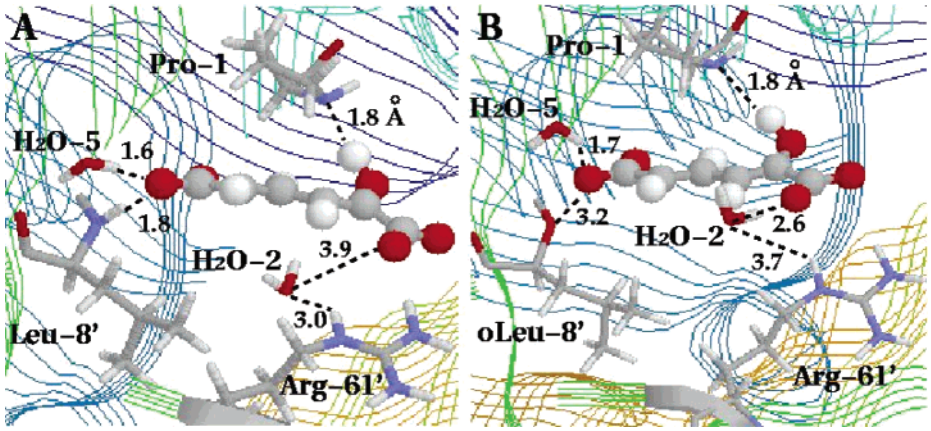

FIGURE 6: Three-dimensional representation of calculated reactant structures for wt-4OT (A) and (OL8)4OT (B).

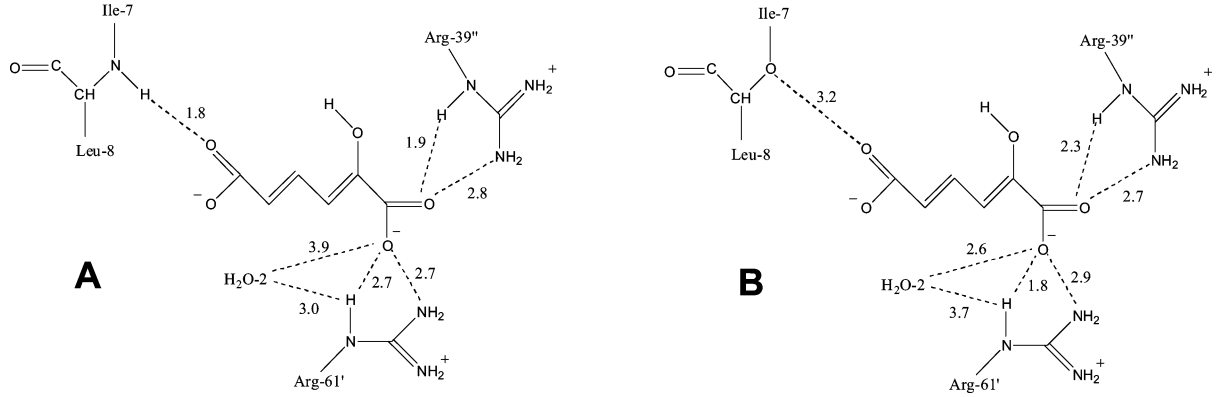

FIGURE 7: Two-dimensional representation of the reactant structures for wt-4OT (A) and (OL8)4OT (B). Only those residues whose orientation in the active site was changed upon mutation are shown.

stabilize the TSs in the wild-type reaction pathway, whereas it does stabilize the TSs of the (OL8)4OT reaction. Significantly, the predicted nonexistent role of Arg-61 in the reaction pathway of the wild-type enzyme is consistent with the results of earlier mutational studies on 4OT in which Arg-61 was replaced with Ala (*12b*). This mutation did not have a measurable effect on 4OT's catalytic properties. Moreover, the predicted contribution of Arg-61 to the reaction pathway of (OL8)4OT is consistent with the experimental results obtained in this work on (OL8)4OT-(R61A). The Arg-61 to Ala mutation in this analogue did have a measurable effect on the catalytic properties of (OL8)-4OT.

In conclusion, our results suggest that the backbone of 4OT plays a significant role in enzyme catalysis. QM/MM calculations show that interactions involving the NH group of Leu-8 lower the energy barrier of the enzymatic reaction, not only through electrostatic contributions but also by forming a H-bond with the substrate in the native structure. Replacement of the NH group of Leu-8 with an O atom deletes this H-bond and destabilizes the TSs. The $\Delta\Delta G^{\ddagger}$ value we determined by experiment for (OL8)4OT was also in good agreement with the $\Delta\Delta E$ value we obtained in our theoretical calculations. Moreover, our experimental results on the synthesis and characterization of (OL8)4OT(R61A) served to confirm the new catalytic role of Arg-61 in (OL8)-4OT that was predicted in our qualitative calculations of the residue-specific, electrostatic contributions to TS stabilization.

ACKNOWLEDGMENT

Computing time from the North Carolina Supercomputing Center was used.

SUPPORTING INFORMATION AVAILABLE

RCDM paths, additional residue analysis, energy barriers, and frequencies for stationary points. This material is available free of charge via the Internet at http://pubs.acs.org.

REFERENCES

1. (a) Dill, K. A. (1990) Dominant forces in protein folding, *Biochemistry 29*, 7133−7135. (b) Pace, C. N. (1997) Evaluating contribution of hydrogen bonding and hydrophobic bonding to protein folding, *Methods Enzymol. 259*, 538−554. (c) England, P. N., Zhang, Z., Dougerty, D. A., and Lester, H. A. (1999) Backbone mutations in transmembrane domains of a ligand-gated ion channel: implications for the mechanism of gating, *Cell 96*, 89−98.
2. (a) Torres, R. A., Schiøtt, B., and Bruice, T. C. (1999) Molecular dynamics simulations of ground and transition states for the hydride transfer from formate to NAD^+ in the active site of formate dehydrogenase, *J. Am. Chem. Soc. 121*, 8164−8173. (b) Topf, M., Várnai, P., and Richards, W. G. (2002) Ab initio QM/MM dynamics simulation of the tetrahedral intermediate of serine proteases: insights into the active site hydrogen-bonding network, *J. Am. Chem. Soc. 124*, 14780−14788.
3. (a) Thomas, N. E., Bramson, N., Miller, T. W., and Kaiser, E. T. (1987) Role of enzyme-peptide substrate backbone hydrogen bonding in determining protein kinase substrate specificities, *Biochemistry 26*, 4461−4466. (b) Lu, W., Qasim, M. A., Laskowski, M., Jr., and Kent, S. B. H. (1997) Probing intermolecular main chain hydrogen bonding in serine proteinase-protein inhibitor complexes: chemical synthesis of backbone-engineered turkey ovomucoid third domain, *Biochemistry 36*, 673−679. (c)

Baca, M., and Kent, S. B. H. (2000) Protein backbone engineering through total chemical synthesis: new insight into the mechanism of HIV-1 protease catalysis, *Tetrahedron 56*, 9503−9513. (d) Koh, J. T., Cornish, V. W., and Schultz, P. G. (1997) An experimental approach to evaluating the role of backbone interactions in proteins using unnatural amino acid mutagenesis, *Biochemistry 36*, 11314−11322. (e) Wales, T. E., and Fitzgerald, M. C. (2001) The energetic contribution of backbone-backbone hydrogen bonds to the thermodynamic stability of a hyperstable P22 Arc repressor mutant, *J. Am. Chem. Soc. 123*, 7709−7710. (f) Blankenship, J. W., Balambika, R., and Dawson, P. E. (2002) Probing backbone hydrogen bonds in the hydrophobic core of GCN4, *Biochemistry 41*, 15676−15684. (g) Silinski, P., and Fitzgerald, M. C. (2003) Comparative analysis of two different amide-to-ester bond mutations in the β-sheet of 4-oxalocrotonate tautomerase, *Biochemistry 42*, 6620−6630.

4. Whitman, C. P., Aird, B. A., Gillespie, W. R., and Stolowich, N. J. (1991) Chemical and enzymatic ketonization of 2-hydroxymuconate, a conjugated enol, *J. Am. Chem. Soc. 113*, 3154−3162.
5. Cisneros, G. A., Liu, H., Zhang, Y., and Yang, W. (2003) *Ab Initio* QM/MM study shows there is no general acid in the reaction catalyzed by 4-oxalocrotonate tautomerase, *J. Am. Chem. Soc. 125*, 10384−10393.
6. Roper, D. I., Subramanya, H. S., Shingler, V., and Wigley, D. B. (1994) Preliminary crystallographic analysis of 4-oxalocrotonate tautomerase reveals the oligomeric structure, *J. Mol. Biol. 243*, 799−801.
7. Waddell, W. J. (1956) A simple ultraviolet spectrophotometric method for the determination of protein, *J. Lab. Clin. Med. 48*, 311−314.
8. Schnolzer, M., Alewoood, P., Jones, A., Alewood, C., and Kent, S. B. H. (1992) *In situ* neutralization in Boc chemistry solid phase peptide synthesis: rapid high-yield assembly of difficult sequences, *Int. J. Pept. Protein Res. 40*, 180−195.
9. (a) Frisch, M. J., Trucks, G. W., Schlegel, H. B., Scuseria, G. E., Robb, M. A., Cheeseman, J. R., Zakrzewski, V. G., Montgomery, J. A., Stratmann, R. E., Burant, J. C., Dapprich, S., Millam, J. M., Daniels, A. D., Kudin, K. N., Strain, M. C., Farkas, O., Tomasi, J., Barone, V., Cossi, M., Cammi, R., Mennucci, B., Pomelli, C., Adamo, C., Clifford, S., Ochterski, J., Petersson, G. A., Ayala, P. Y., Cui, Q., Morokuma, K., Malick, D. K., Rabuck, A. D., Raghavachari, K., Foresman, J. B., Cioslowski, J., Ortiz, J. V., Stefanov, B. B., Liu, G., Liashenko, A., Piskorz, P., Komaromi, I., Gomperts, R., Martin, R. L., Fox, D. J., Keith, T., Al-Laham, M. A., Peng, C. Y., Nanayakkara, A., Gonzalez, C., Challacombe, M., Gill, P. M. W., Johnson, B., Chen, W., Wong, M. W., Andres, J. L., Head-Gordon, M., Replogle, E. S., and Pople, J. A. (1998) *Gaussian 98*, revision A5, Gaussian Inc., Pittsburgh, PA. (b) Ponder, J. (1998) *TINKER, Software Tools for Molecular Design*, version 3.6, Washington University, St. Louis (the most updated version of *Tinker* can be obtained from http://dasher.wustl.edu/tinker). (c) Zhang, Y., Liu, H., and Yang, W. (2000) Free energy calculation on enzyme reactions with an efficient iterative procedure to determine minimum energy paths on a combined QM/MM potential energy surface, *J. Chem. Phys. 112*, 3483−3492.
10. Williams, I., and Maggiora, G. (1982) Use and abuse of the distinguished-coordinate method for transition-state structure searching, *J. Mol. Struct. 89*, 365.
11. Fitzgerald, M. C., Chernushivech, I., Standing, K. G., Whitman, C. P., and Kent, S. B. H. (1996) Probing the oligomeric structure of an enzyme by electrospray ionization time-of-flight mass spectrometry, *Proc. Natl. Acad. Sci. U.S.A. 93*, 6851−6856.
12. (a) Harris, T. K., Czerwinski, R. M., Johnson, W. H., Jr., Legler, P. M., Stivers, J. T., Mildvan, A. S., and Whitman, C. P. (1999) Effects of mutations of the active site arginine residues in 4-oxalocrotonate tautomerase on the pK_a values of active site residues and on the pH dependence of catalysis, *Biochemistry 38*, 12358−12366. (b) Harris, T. K., Czerwinski, R. M., Johnson, W. H., Legler, P. M., Abeygunawardana, C., Massiah, M. A., Stivers, J. T., Whitman, C. P., and Mildvan, A. S. (1999) Kinetic, stereochemical and structural effects of mutations of the active site arginine residues in 4-oxalocrotonate tautomerase, *Biochemistry 38*, 12343−12357.
13. Silinski, P. (2003) Understanding the role of backbone-backbone hydrogen bonding in the folding and stability of the hexameric enzyme 4-oxalocrotonate tautomerase (4OT), Ph.D. Thesis, Duke University, Durham, NC.

BI049943P